The current issue and full text archive of this journal is available at
www.emeraldinsight.com/0961-5539.htm

Application of high-order spatial resolution schemes to the hybrid finite volume/finite element method for radiative transfer in participating media

Received 5 December 2005
Revised 2 January 2007
Accepted 2 January 2007

P.J. Coelho and D. Aelenei
Mechanical Engineering Department, Instituto Superior Técnico, Technical University of Lisbon, Lisboa, Portugal

Abstract

Purpose – This paper sets out to implement bounded high-order (HO) resolution schemes in a hybrid finite volume/finite element method for the solution of the radiative transfer equation.

Design/methodology/approach – The hybrid finite volume/finite element method had formerly been developed using the step scheme, which is only first-order accurate, for the spatial discretization. Here, several bounded HO resolution schemes, namely the MINMOD, CLAM, MUSCL and SMART schemes, formulated using the normalized variable diagram, were implemented using the deferred correction procedure.

Findings – The results obtained reveal an interaction between spatial and angular discretization errors, and show that the HO resolution schemes yield improved accuracy over the step scheme if the angular discretization error is small.

Research limitations/implications – Although the HO resolution schemes reduce the spatial discretization error, they do not influence the angular discretization error. Therefore, the global error is only reduced if the angular discretization error is also small.

Practical implications – The use of HO resolution schemes is only effective if the angular refinement yields low-angular discretization errors. Moreover, spatial and angular refinement should be carried out simultaneously.

Originality/value – The paper extends a methodology formerly developed in computational fluid dynamics, and aimed at the improvement of the solution accuracy, to the hybrid finite volume/finite element method for the solution of the radiative transfer equation.

Keywords Heat transfer, Finite volume methods, Finite element analysis

Paper type Research paper

Nomenclature

A_k	= area of a cell face normal to the kth direction (m^2)	D_{ln}	= coefficients of matrix **D** (equation (6d))
$A_{mn,k}$	= coefficients of matrix **A** (equation (6a))	E	= number of control angle elements; absolute error
B_{mn}	= coefficients of matrix **B** (equation (6b))	I	= radiation intensity ($W\ m^{-2}\ sr^{-1}$)
C_m	= coefficients of vector **C** (equation (6c))	K	= number of spatial dimensions

This work was developed within the framework of project POCTI/EME/44107/2002, which is financially supported by FCT-Fundação para a Ciência e a Tecnologia under the programme POCTI (42.71 per cent of the funds from FEDER and 57.29 per cent from OE).

International Journal of Numerical Methods for Heat & Fluid Flow
Vol. 18 No. 2, 2008
pp. 173-184

0961-5539
DOI 10.1108/09615530810846329

L = distance between the walls (m)
$\mathbf{n}$ = outer unit vector normal to the wall
N = total number of angular nodes
$\mathbf{r}$ = position vector
$\mathbf{s}$ = unit vector in the direction of propagation of radiation
T = temperature (K)
V = volume (m^3)
x_k = coordinate along the kth direction (m)

Greek letters

β = extinction coefficient (m^{-1})
ε = emissivity
κ = absorption coefficient (m^{-1})
μ_k = direction cosine of the kth direction
σ = Stefan-Boltzmann constant (W m^{-2} K^{-4})
σ_s = scattering coefficient (m^{-1})
τ_L = optical thickness of the medium
ϕ = basis function; non-dimensional temperature field
Φ = scattering phase function
ψ = non-dimensional radiative heat flux
Ω = solid angle

Superscripts

dc = deferred correction
e = control angle element
HO = high-order
m = angular node
$\sim$ = normalized variable

Subscripts

b = blackbody
C = central grid node
D = downstream grid node
f = cell face
k = coordinate direction
m = angular node
P = spatial grid node
U = upstream grid node
w = wall

Introduction

Radiative heat transfer is an important heat transfer mode in many combustion systems, including boilers, furnaces, internal combustion and rocket engines, and also in fires. Solar and atmospheric radiation are other important application areas. Many radiation models have been developed over the years, such as the Monte Carlo (Howell, 1968), zonal (Hottel and Sarofim, 1967), spherical harmonics (Mengüç and Viskanta, 1985), discrete transfer (Lockwood and Shah, 1981), discrete ordinates (Fiveland, 1984) and finite volume (Raithby and Chui, 1990) methods. Recently, a new hybrid model has been developed that combines features of the finite volume and finite element methods. The method was referred to as HYDRA, which stands for hybrid finite volume/finite element discretization method for the solution of the radiative transfer equation (RTE), or in short, hybrid discretization for radiation (Coelho, 2005a, b). The method may be applied to both grey and non-grey media, non-scattering and scattering media, simple and complex geometries. However, only radiative transfer in rectangular enclosures with grey, emitting-absorbing and scattering media has been studied so far.

In the HYDRA method, the spatial and angular dependence of the radiation intensity are split in such a way that the radiation intensity is approximated by a linear combination of basis functions dependent only on the angular direction. The coefficients of the approximation are functions of the spatial coordinates. The basis functions are linearly independent functions, which are prescribed according to criteria used in the finite element method. The angular discretization is carried out in such a way that either the polar or the azimuthal angle remains constant along the boundaries of the elements. This means that a classical polar/azimuthal discretization is carried out, like in the finite volume method (FVM) and discrete transfer method (DTM) method. However, in these methods the radiation intensity is constant over a control angle or over a solid angle, respectively. Similarly, in the discrete ordinates method (DOM), the RTE is solved for a set of discrete directions that span the total solid angle

of 4π, and the integrals over that solid angle are replaced by numerical quadratures. The radiation intensity is taken as constant for all directions related to a quadrature weight. Therefore, the radiation intensity in the FVM, DTM and DOM is a directional discontinuous function. On the contrary, in the present method the radiation intensity is a continuously varying function, because the basis functions vary continuously within the control angle elements, as well as across their boundaries. Bilinear basis functions were chosen for the angular discretization.

The spatial discretization is performed using the FVM. Formerly, the step scheme was employed to relate the cell face radiation intensities to the central grid node radiation intensity (Coelho, 2005a, b). However, it is well known that the step scheme, which is the counterpart of the well-known upwind scheme in computational fluid dynamics (CFD), is only first order accurate, and causes numerical smearing. In this paper, high-order (HO) resolution schemes are applied to the spatial discretization, and two radiative heat transfer problems in enclosures with a grey medium are solved.

Radiation model

The RTE for an emitting, absorbing and scattering grey medium may be written as:

$$\sum_{k=1}^{K} \mu_k(\mathbf{s}) \frac{\partial I(\mathbf{r},\mathbf{s})}{\partial x_k} = -\beta I(\mathbf{r},\mathbf{s}) + \kappa I_\mathrm{b}(\mathbf{r}) + \frac{\sigma_\mathrm{s}}{4\pi} \int_{4\pi} I(\mathbf{r},\mathbf{s}')\Phi(\mathbf{s}',\mathbf{s})\mathrm{d}\Omega' \tag{1}$$

The spatial and angular dependence of the radiation intensity are split as:

$$I(\mathbf{r},\mathbf{s}) = \sum_{m=1}^{N} I^m(\mathbf{r})\phi_m(\mathbf{s}) \tag{2}$$

where m stands for an angular node, as defined below. Inserting equation (2) into equation (1) yields:

$$\begin{aligned} \sum_{k=1}^{K} \mu_k(\mathbf{s}) \left(\sum_{m=1}^{N} \phi_m(\mathbf{s}) \frac{\partial I^m(\mathbf{r})}{\partial x_k} \right) = & -\beta \sum_{m=1}^{N} I^m(\mathbf{r})\phi_m(\mathbf{s}) + \kappa I_\mathrm{b}(\mathbf{r}) \\ & + \frac{\sigma_\mathrm{s}}{4\pi} \sum_{l=1}^{N} I^l(\mathbf{r}) \int_{4\pi} \phi_l(\mathbf{s}')\Phi(\mathbf{s}',\mathbf{s})\mathrm{d}\Omega' \end{aligned} \tag{3}$$

Multiplying both terms of this equation by the basis function ϕ_n and integrating over all directions, the following set of N simultaneous integro-differential equations is obtained:

$$\begin{aligned} & \sum_{k=1}^{K} \int_{4\pi} \mu_k(\mathbf{s}) \left(\sum_{m=1}^{N} \phi_m(\mathbf{s}) \frac{\partial I^m(\mathbf{r})}{\partial x_k} \right) \phi_n(\mathbf{s})\mathrm{d}\Omega \\ & = -\beta \sum_{m=1}^{N} I^m(\mathbf{r}) \int_{4\pi} \phi_m(\mathbf{s})\phi_n(\mathbf{s})\mathrm{d}\Omega + \kappa I_\mathrm{b}(\mathbf{r}) \int_{4\pi} \phi_n(\mathbf{s})\mathrm{d}\Omega \\ & \quad + \frac{\sigma_\mathrm{s}}{4\pi} \sum_{l=1}^{N} I^l(\mathbf{r}) \int_{4\pi} \int_{4\pi} \phi_l(\mathbf{s}')\Phi(\mathbf{s}',\mathbf{s})\mathrm{d}\Omega'\phi_n(\mathbf{s})\mathrm{d}\Omega \quad n = 1, 2, \ldots, N \end{aligned} \tag{4}$$

This equation may be written as:

$$\sum_{k=1}^{K}\left(\sum_{m=1}^{N}\frac{\mu_k(\mathbf{s})}{|\mu_k(\mathbf{s})|}\frac{\partial I^m(\mathbf{r})}{\partial x_k}A_{mn,k}\right) = -\beta\sum_{m=1}^{N}I^m(\mathbf{r})B_{mn}+\kappa I_{\mathrm{b}}(\mathbf{r})C_n+\frac{\sigma_{\mathrm{s}}}{4\pi}\sum_{l=1}^{N}I^l(\mathbf{r})D_{ln} \tag{5}$$

where matrices **A**, **B**, **C** and **D** have been introduced for conciseness. Their components are given by:

$$A_{mn,k}=\int_{4\pi}|\mu_k(\mathbf{s})|\phi_m(\mathbf{s})\phi_n(\mathbf{s})\mathrm{d}\Omega \tag{6a}$$

$$B_{mn}=\int_{4\pi}\phi_m(\mathbf{s})\phi_n(\mathbf{s})\mathrm{d}\Omega \tag{6b}$$

$$C_n=\int_{4\pi}\phi_n(\mathbf{s})\mathrm{d}\Omega \tag{6c}$$

$$D_{ln}=\int_{4\pi}\int_{4\pi}\phi_l(\mathbf{s}')\Phi(\mathbf{s}',\mathbf{s})\mathrm{d}\Omega'\phi_n(\mathbf{s})\mathrm{d}\Omega \tag{6d}$$

Equation (5) is discretized in space using the FVM in a Cartesian coordinate frame. Integrating equation (5) over a control volume and applying the Gauss divergence theorem yields the following equation:

$$\sum_{k=1}^{K}\left(\sum_{m=1}^{N}\left(I^m_{\mathrm{out},k}-I^m_{\mathrm{in},k}\right)A_k A_{mn,k}\right) = -\beta V\sum_{m=1}^{N}I^m_{\mathrm{P}}B_{mn}+\kappa V I_{\mathrm{b,P}}C_n+\frac{\sigma_{\mathrm{s}}}{4\pi}V\sum_{l=1}^{N}I^l_{\mathrm{P}}D_{ln} \tag{7}$$

A spatial discretization scheme is needed to relate the radiation intensity entering, I_{in}, or leaving, I_{out}, a cell face to the radiation intensity at the grid node, I_{P}. The mth coefficient of the mean radiation intensity at cell face k is calculated using a HO discretization scheme. This is implemented using the deferred correction procedure (Khosla and Rubin, 1974), as follows:

$$I^m_k=\left(I^m_k\right)^{\mathrm{step}}+\left[\left(I^m_k\right)^{\mathrm{HO}}-\left(I^m_k\right)^{\mathrm{step}}\right]=\left(I^m_k\right)^{\mathrm{step}}+\left(I^m_k\right)^{\mathrm{dc}} \tag{8}$$

where the superscripts "step" and "dc" stand for the step scheme and for the deferred correction intensity, respectively. The radiation intensity at a cell face and leaving a control volume, evaluated according to the step scheme, is equal to the radiation intensity at that control volume, i.e.:

$$\left(I^m_{\mathrm{out},k}\right)^{\mathrm{step}}=I^m_{\mathrm{P}} \tag{9}$$

Therefore, we may write:

$$I^m_{\mathrm{out},k} = I^m_{\mathrm{P}} + \left(I^m_{\mathrm{out},k}\right)^{\mathrm{dc}} \tag{10}$$

Inserting these expressions into equation (7) yields:

$$\begin{aligned}\sum_{k=1}^{K}\left[\sum_{m=1}^{N}\left(I^m_{\mathrm{P}} - \left(I^m_{\mathrm{in},k}\right)^{\mathrm{step}} + \left(I^m_{\mathrm{out},k} - I^m_{\mathrm{in},k}\right)^{\mathrm{dc}}\right)A_k A_{mn,k}\right] \\ = -\beta V\sum_{m=1}^{N} I^m_{\mathrm{P}} B_{mn} + \kappa V I_{\mathrm{b,P}} C_n + \frac{\sigma_{\mathrm{s}}}{4\pi} V\sum_{l=1}^{N} I^l_{\mathrm{P}} D_{ln}\end{aligned} \tag{11}$$

which may be rewritten as:

$$\begin{aligned}\sum_{m=1}^{N}\left[\left(\sum_{k=1}^{K} A_k A_{mn,k}\right) + \beta V B_{mn}\right] I^m_{\mathrm{P}} = \sum_{k=1}^{K}\sum_{m=1}^{N}\left(I^m_{\mathrm{in},k}\right)^{\mathrm{step}} A_k A_{mn,k} + \kappa V I_{\mathrm{b,P}} C_n \\ + \frac{\sigma_{\mathrm{s}}}{4\pi} V\sum_{l=1}^{N} I^l_{\mathrm{P}} D_{ln} - \sum_{k=1}^{K}\sum_{m=1}^{N}\left(I^m_{\mathrm{out},k} - I^m_{\mathrm{in},k}\right)^{\mathrm{dc}} A_k A_{mn,k}\end{aligned} \tag{12}$$

If the step scheme is used, the last term on the right side is equal to zero and this equation reverts to that derived in Coelho (2005a). If a HO scheme is employed, the last term, which is treated explicitly, is non-zero.

The angular discretization is carried out as described in Coelho (2005a, b). The solid angle of 4π around a grid node is discretized by means of lines of constant latitude and longitude. The angular region limited by two adjacent lines of constant latitude and two adjacent lines of constant longitude is referred to as a control angle element. The points of intersection between lines of constant latitude and lines of constant longitude are referred to as angular nodes. The basis functions are defined piecewise element by element and are taken as a bilinear function over every control angle element. The mth basis function is equal to 1 at the mth angular node and 0 at all the other angular nodes ($1 \leq m \leq N$). The restriction of a basis function to a control angle element is referred to as shape function and denoted by ψ. In this way, only four of the N basis functions are different from 0 over a given control angle element, thus yielding four shape functions defined over every control angle element Ω_{e}. The calculation of the coefficients of matrices **A**, **B**, **C** and **D** is carried out element by element, as in the finite element method. The coefficients of the local element matrices are evaluated analytically, except the coefficients of matrix **D**, which may require numerical integration, depending on the scattering phase function. The local element matrices are assembled to obtain the global matrices. Details of this procedure are given in Coelho (2005a, b).

The incident radiation at a grid node and the incident heat flux at a boundary are also calculated element by element, as described in Coelho (2005a, b).

High-order resolution schemes

The spatial discretization of the term on the left side of the RTE, equation (1), requires the calculation of the radiation intensity at the cell faces of a control volume. This calculation may be accomplished using many different discretization schemes.

A review of the schemes used in the DOM and FVMs for the solution of the RTE was presented in Chai *et al.* (1994). In that work, it was argued that none of the available schemes was satisfactory, and the step scheme was recommended, because of its stability and boundedeness properties. Still, this is a first-order scheme, which is the counterpart of the upwind scheme in CFD. It is well known that this scheme is prone to false diffusion, a shortcoming that is also shared by the RTE, as discussed by Chai *et al.* (1993).

More recently, it was realized that the spatial discretization of the term on the left of the RTE is similar to the discretization of the convective term of the momentum equations in CFD. Therefore, the discretization schemes developed in CFD may also be applied to the RTE. In particular, bounded HO resolution schemes, such as, for example, the MINMOD, CLAM, MUSCL and SMART schemes, may also be used in radiative transfer. Formerly, these schemes were applied in the framework of the DOM (Jessee and Fiveland, 1997). Here, we will apply these schemes to the recently developed HYDRA method.

Bounded HO resolution schemes may be formulated using the diagram of normalized variables, as described by Leonard (1997). A normalized radiation intensity, denoted with a tilde, is defined as follows:

$$\tilde{I} = \frac{I - I_{\mathrm{U}}}{I_{\mathrm{D}} - I_{\mathrm{U}}} \tag{13}$$

where subscripts U and D identify the grid nodes associated with the upstream and downstream control volumes, respectively. Denoting by f the cell face of a control volume where we want to compute the radiation intensity and by C the grid node associated with that control volume, the functional relationships for the schemes mentioned above are as follows (Darwish, 1993):

MINMOD:

$$\tilde{I}_{\mathrm{f}} = \begin{cases} 1.5\tilde{I}_{\mathrm{C}} & \text{if } 0 < \tilde{I}_{\mathrm{C}} < 0.5 \\ 0.5(1 + \tilde{I}_{\mathrm{C}}) & \text{if } 0.5 < \tilde{I}_{\mathrm{C}} < 1 \\ \tilde{I}_{\mathrm{C}} & \text{elsewhere} \end{cases} \tag{14}$$

CLAM:

$$\tilde{I}_{\mathrm{f}} = \begin{cases} \tilde{I}_{\mathrm{C}}(2 - \tilde{I}_{\mathrm{C}}) & \text{if } 0 < \tilde{I}_{\mathrm{C}} < 1 \\ \tilde{I}_{\mathrm{C}} & \text{elsewhere} \end{cases} \tag{15}$$

MUSCL:

$$\tilde{I}_{\mathrm{f}} = \begin{cases} 2\tilde{I}_{\mathrm{C}} & \text{if } 0 < \tilde{I}_{\mathrm{C}} < 1/4 \\ 0.25 + \tilde{I}_{\mathrm{C}} & \text{if } 1/4 < \tilde{I}_{\mathrm{C}} < 3/4 \\ 1 & \text{if } 3/4 < \tilde{I}_{\mathrm{C}} < 1 \\ \tilde{I}_{\mathrm{C}} & \text{elsewhere} \end{cases} \tag{16}$$

SMART:

$$\tilde{I}_f = \begin{cases} 3\tilde{I}_C & \text{if } 0 < \tilde{I}_C < 1/6 \\ (3/8) + (3\tilde{I}_C/4) & \text{if } 1/6 < \tilde{I}_C < 5/6 \\ 1 & \text{if } 5/6 < \tilde{I}_C < 1 \\ \tilde{I}_C & \text{elsewhere} \end{cases} \quad (17)$$

These relationships are restricted to uniform grids, but may be generalized for non-uniform grids (Darwish and Moukalled, 1994).

Results and discussion

One-dimensional isotropically scattering medium

The first test problem consists of a plane medium bounded by two parallel and infinitely long walls. The medium neither absorbs nor emits, but scatters isotropically. Hence, the scattering albedo is equal to one. The walls are maintained at a prescribed temperature. The analytical solution is available (Heaslet and Warming, 1965). The non-dimensional radiative heat flux, ψ, is given by:

$$\psi = \frac{q_w}{\sigma\left(T_{w,1}^4 - T_{w,2}^4\right)} = \frac{\psi_b}{1 + \psi_b((1/\varepsilon_1) + (1/\varepsilon_2 - 2))} \quad (18)$$

where the indices 1 and 2 refer to the walls, and ψ_b, is given by:

$$\psi_b = 1 - 2\int_0^{\tau_L} \phi_b(\tau')E_2(\tau')d\tau' \quad (19)$$

Here, $E_n(x)$ stands for the exponential integral function of order n and ϕ_b is the non-dimensional temperature field for black walls, which may be evaluated from the solution of the following equation:

$$\phi_b(\tau) = \frac{1}{2}\left[E_2(\tau) + \int_0^{\tau_L} \phi_b(\tau')E_1(|\tau - \tau'|)d\tau'\right] \quad (20)$$

Both ψ and ψ_b are independent of the temperature of the walls, and ψ_b is independent of the emissivity of the walls.

The results of the calculations performed using 20 control volumes and 2×2, 3×3, 4×4, 5×5 and 6×6 (4, 9, 16, 25 and 36, respectively) control angle elements per octant are shown in Figure 1. The walls are black in Figure 1(a) and (b) and grey, with $\varepsilon_1 = 0.8$ and $\varepsilon_2 = 0.5$, in Figure 1(c) and (d). Calculations were performed for optical thicknesses, based on the distance to the walls, of 0.1, 0.5, 1.0 and 5.0, but only the results for $\tau_L = 0.1$ and $\tau_L = 5.0$ are reported here. It can be seen that the results are qualitatively similar in both cases.

The predicted non-dimensional radiative heat flux is approximately independent of the discretization scheme in the case of an optically thin medium ($\tau_L = 0.1$), and the numerical solution tends to the analytical one as the number of control angle elements increases. Notice that, in the limit of a transparent medium ($\tau_L = 0$), the radiation intensity along a given direction would be constant, and all the schemes would give

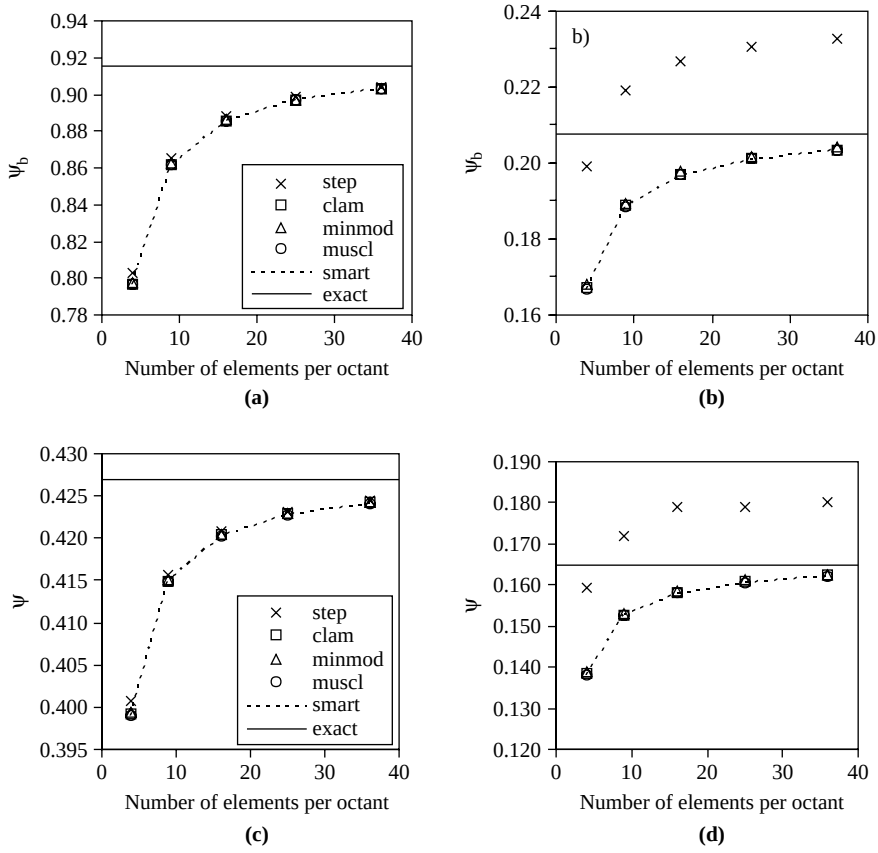

Figure 1.
Non-dimensional radiative heat flux in a one-dimensional isotropically scattering medium bounded by two parallel infinitely long walls (a) black walls, $\tau_L = 0.1$; (b) black walls, $\tau_L = 5.0$; (c) grey walls, $\tau_L = 0.1$; (d) grey walls, $\tau_L = 5.0$

exactly the same solution. Therefore, a crude discretization scheme, like the step scheme, performs satisfactorily, and no visible increase in accuracy results from using HO schemes.

In the case of an optically thick medium, the radiation intensity changes along the direction of propagation, but slowly. The step scheme performs well for a small number of control angle elements, but the solution accuracy decreases if that number increases. This reveals that the lower error observed for a small number of angular elements is not due to a low-spatial discretization error, but rather due to a compensation between spatial and angular discretization errors, which have opposite effects. This compensation effect between spatial and angular discretization errors was formerly discussed by Raithby (1999) in the framework of the FVM, and by Coelho (2002) for the DOM. In these three methods for the solution of the RTE, namely HYDRA, FVM and DOM, the spatial discretization is performed using finite volumes. The angular discretization differs, such that the finite element method is used in HYDRA, the FVM is used in the FVM, and an S_N quadrature is generally used in the DOM, although other alternatives are available. However, in these three methods, the opposite effects of spatial and angular discretization errors have been observed. If the number of control

angle elements increases, the angular discretization error becomes smaller, and no longer compensates the spatial discretization error of the step scheme, which becomes dominant. Accordingly, the solution error increases.

If HO discretization schemes are used, the solution error is large for a small number of control angle elements, because the spatial discretization error is small, but the angular discretization error is large. The angular refinement improves the solution accuracy. The difference between the various HO discretization schemes is hardly visible for this test case.

The computational requirements increase with the increase of the optical thickness of the medium, and they are higher for grey walls than for black ones. The HO resolution schemes yield an increase of the CPU time by a factor of 2.5 up to 7 compared with the STEP scheme, depending on the optical thickness of the medium and on the angular discretization. This increase is mainly due to the slower convergence rate of the HO resolution schemes, which implies more iterations to attain the same convergence criterion. In the case of optically thin media ($\tau_L = 0.1$), that factor is about 7 for 2×2 control angle elements per octant, and decreases up to about 4 for 6×6 control angle elements per octant. In the case of optically thick media ($\tau_L = 5.0$), the CPU time of HO resolution schemes is about three times higher than that of the STEP scheme for 2×2 control angle elements per octant, and decreases to about 2.5 times higher for 6×6 control angle elements per octant. The emissivity of the boundaries has only a marginal influence on these factors.

The computational requirements of the different HO resolution schemes are about the same for all of them, the MINMOD being marginally more economical than the others, and the SMART slightly more computationally intensive. From these results, it can be concluded that the use of HO resolution schemes for the present test case only pays off in the case of optically thick media.

Two-dimensional isotropically scattering medium

The previous test case was one-dimensional, and so only streamwise diffusion was present. In multidimensional problems, when gradients of the transported variable exist perpendicular to the transport direction and this direction is oblique to the grid lines, crosswise diffusion takes place in addition to streamwise diffusion.

A two-dimensional square enclosure with black walls is considered here. The medium scatters isotropically, and there is neither emission nor absorption. Notice that this is equivalent to an emitting-absorbing and non-scattering medium in radiative equilibrium. The optical thickness of the medium is equal to one. The top boundary is hot, with an emissive power of unity, while the other boundaries are cold. The quasi-exact solution reported in Crosbie and Schrenker (1984) is taken as the reference solution.

The calculations were carried out using a 10×10 uniform grid and 2×2, 3×3, 4×4, 5×5 and 6×6 control angle elements per octant. Figure 2 shows the mean absolute error of the boundary heat flux and radiative heat source as a function of the number of control angle elements per octant.

If the step scheme is used, the solution error firstly decreases, and then increases with the angular refinement, except for the heat flux at the side wall, whose error continuously increases. This behaviour is again a consequence of the interaction between spatial and angular discretization errors. If both the spatial and angular discretizations are coarse, the error compensation may yield relatively small errors, but

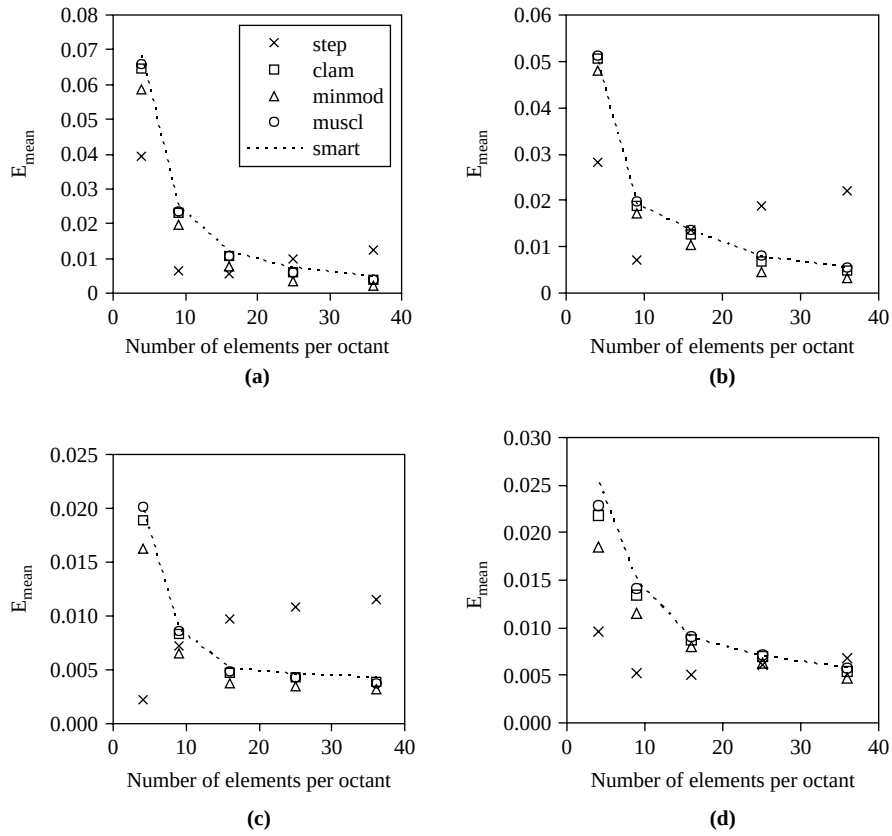

Figure 2.
Mean absolute error
(a) normalized heat flux at the top boundary;
(b) normalized heat flux at the bottom boundary;
(c) normalized heat flux along the side boundary;
(d) source function along the symmetry plane of the enclosure

as the angular refinement takes place, the large spatial discretization error is no longer compensated and contributes to increase the solution error.

The HO resolution schemes yield larger errors than the step scheme for a coarse angular discretization. In fact, although the HO resolution schemes are more accurate, and yield a lower spatial discretization error than the step scheme, the angular discretization error is large for a coarse angular discretization, and is responsible for a higher solution error. If the step scheme is used, then both high spatial and angular discretization errors are present, but since they have opposite effects, there is an error compensation that justifies the smaller solution error in comparison with the HO schemes. When the number of control angle elements increases, the lower spatial error of the HO schemes along with the decrease of the angular discretization error yields a continuous decrease of the solution error. Therefore, for a sufficiently fine angular discretization, HO schemes perform better than the step scheme. The difference between the various HO schemes is visible, but marginal.

As in the previous test case, the CPU time needed to achieve convergence is greater for the HO resolution schemes than for the STEP scheme. The ratio of the CPU time of the HO resolution schemes to the CPU time of the STEP scheme ranges from about 2, in the case of 6×6 control angle elements per octant, to about 5 in the case of only 2×2

control angle elements per octant. As an example, the CPU time for the CLAM scheme with 4×4 control angle elements per octant is similar to that of the STEP scheme with 5×5 control angle elements. Since, the accuracy of the CLAM scheme is better than that of the STEP scheme with such angular discretizations, the use of high-resolution schemes is recommended.

Although only purely scattering media have been considered in the two test cases presented here, other test cases reported in Coelho (2005a, b, 2006) demonstrate the suitability of the HYDRA method for the full range of scattering albedos from 0 to 1, as well as for optical thickness ranging from 0.1 to 1.0, and for either grey or black boundary surfaces. Moreover, a comparison of the accuracy of the HYDRA method with the DOM using either the STEP scheme or HO spatial resolution schemes has recently been reported in Coelho (2006).

So far, only rectangular geometries have been simulated. The extension of the present method to irregular geometries is in progress, and should not present any major problems. It is also expected to observe the same trend of error in irregular geometries, but this is subject to future confirmation.

Conclusion

Several HO resolution schemes have been applied to the spatial discretization of a hybrid finite volume/finite element method for the solution of the RTE in enclosures with a grey medium, and compared with the step scheme. The results reveal an interaction between spatial and angular discretization errors, and show that the HO resolution schemes yield improved accuracy over the step scheme if the angular discretization error is small.

References

Chai, J.C., Lee, H.S. and Patankar, S.V. (1993), "Ray effect and false scattering in the discrete ordinates method", *Numerical Heat Transfer. Part B: Fundamentals*, Vol. 24, pp. 373-89.

Chai, J.C., Patankar, S.V. and Lee, H.S. (1994), "Evaluation of spatial differencing practices for the discrete-ordinates method", *Journal of Thermophysics and Heat Transfer*, Vol. 8, pp. 140-4.

Coelho, P.J. (2002), "The role of ray effects and false scattering on the accuracy of the standard and modified discrete ordinates methods", *Journal of Quantitative Spectroscopy and Radiative Transfer*, Vol. 73, pp. 231-8.

Coelho, P.J. (2005a), "A hybrid finite volume/finite element discretization method for the solution of the radiative transfer equation", *Journal of Quantitative Spectroscopy and Radiative Transfer*, Vol. 93, pp. 89-101.

Coelho, P.J. (2005b), "Fundamentals of a new method for the solution of the radiative transfer equation", *International Journal of Thermal Sciences*, Vol. 44, pp. 809-21.

Coelho, P.J. (2006), "Assessment of the accuracy of the hybrid finite element/finite volume method for the solution of the radiative transfer equation", paper presented at 13th Int. Heat Transfer Conference, Sydney, 13-18 August.

Crosbie, L. and Schrenker, R.G. (1984), "Radiative transfer in a two-dimensional rectangular medium exposed to diffuse radiation", *Journal of Quantitative Spectroscopy and Radiative Transfer*, Vol. 31, pp. 339-72.

Darwish, M.S. (1993), "A new high-resolution scheme based on the normalized variable formulation", *Numerical Heat Transfer. Part B: Fundamentals*, Vol. 24, pp. 353-71.

Darwish, M.S. and Moukalled, F.H. (1994), "Normalized variable and space formulation for high-resolution schemes", *Numerical Heat Transfer. Part B: Fundamentals*, Vol. 26, pp. 79-96.

Fiveland, W.A. (1984), "Discrete-ordinates solution of the radiative transport equation for rectangular enclosures", *Journal of Heat Transfer*, Vol. 106, pp. 699-706.

Heaslet, M. and Warming, R. (1965), "Radiative transfer and wall temperature slip in an absorbing planar medium", *International Journal of Heat and Mass Transfer*, Vol. 8, pp. 979-94.

Hottel, H.C. and Sarofim, A.F. (1967), *Radiative Transfer*, McGraw-Hill, New York, NY.

Howell, J.R. (1968), "Application of Monte Carlo to heat transfer problems", in Hartnett, J.P. and Irvine, T. (Eds), *Advances in Heat Transfer*, Vol. 5, Academic Press, New York, NY.

Jessee, J.P. and Fiveland, W.A. (1997), "Bounded, high-resolution differencing schemes applied to the discrete ordinates method", *Journal of Thermophysics and Heat Transfer*, Vol. 11, pp. 540-8.

Khosla, P.K. and Rubin, S.G. (1974), "A diagonally dominant second order accurate implicit scheme", *Computers & Fluids*, Vol. 2, pp. 207-9.

Leonard, B.P. (1997), "Bounded higher-order upwind multidimensional finite-volume convection-diffusion algorithms", in Minkowycz, W.J. and Sparrow, E.M. (Eds), *Advances in Numerical Heat Transfer*, Vol. 1, Taylor & Francis, New York, NY, pp. 1-57.

Lockwood, F.C. and Shah, N.G. (1981), "A new radiation solution method for incorporation in general combustion prediction procedures", paper presented at 18th Symposium (Int.) on Combustion. The Combustion Institute, Pittsburgh, pp. 1405-14.

Mengüç, M.P. and Viskanta, R. (1985), "Radiative transfer in three-dimensional rectangular enclosures containing inhomogeneous, anisotropically scattering media", *Journal of Quantitative Spectroscopy and Radiative Transfer*, Vol. 33, pp. 533-49.

Raithby, G.D. (1999), "Evaluation of discretization errors in finite-volume radiant heat transfer predictions", *Numerical Heat Transfer, Part B: Fundamentals*, Vol. 36, pp. 241-64.

Raithby, G.D. and Chui, E.H. (1990), "A finite-volume method for predicting a radiant heat transfer in enclosures with participating media", *Journal of Heat Transfer*, Vol. 112, pp. 415-23.

Corresponding author
P. J. Coelho can be contacted at: pedro.coelho@ist.utl.pt